

Manifestation of nematic degrees of freedom in the Raman response function of iron pnictides

U. Karahasanovic,^{1,2} F. Kretzschmar,^{3,4} T. Böhm,^{3,4} R. Hackl,³ I. Paul,⁵ Y. Gallais,⁵ and J. Schmalian^{1,2}

¹*Institut für Theorie der Kondensierten Materie, Karlsruher Institut für Technologie, DE-76131 Karlsruhe, Germany*

²*Institut für Festkörperphysik, Karlsruher Institut für Technologie, DE-76131 Karlsruhe, Germany*

³*Walther Meissner Institut, Bayerische Akademie der Wissenschaften, 85748 Garching, Germany*

⁴*Fakultät für Physik E23, Technische Universität München, 85748 Garching, Germany*

⁵*Laboratoire Matériaux et Phénomènes Quantiques, UMR 7162 CNRS,*

Université Paris Diderot, Bat. Condorcet 75205 Paris Cedex 13, France

(Dated: June 14, 2021)

We establish a relation between the Raman response function in the B_{1g} channel and the electronic contribution to the nematic susceptibility within the spin-driven approach to electron nematicity of the iron based superconductors. The spin-driven nematic phase, characterized by the broken C_4 symmetry, but unbroken $O(3)$ spin-rotational symmetry, is generated by the presence of magnetic fluctuations associated with the striped phase. It occurs as a separate phase between T_m and T_s in systems where the structural and magnetic phase transitions are separated. Detecting the presence of nematic degrees of freedom in iron-based superconductors is a difficult task, since it involves measuring higher order spin correlation functions. We show that the nematic degrees of freedom manifest themselves in the experimentally measurable Raman response function. We calculate the Raman response function in the tetragonal phase in the large N limit by considering higher-order Aslamazov-Larkin type of diagrams. They are characterized by a series of inserted quartic paramagnon couplings mediated by electronic excitations that resemble the nematic coupling constant of the theory. These diagrams effectively account for collisions between spin fluctuations. By summing an infinite number of such higher order diagrams, we demonstrate that the electronic Raman response function shows a clear maximum at the structural phase transition in the B_{1g} channel. Hence, the Raman response function can be used to probe nematic degrees of freedom.

PACS numbers: 74.25.nd, 74.70.Xa, 74.20.Mn, 74.25.Ha

I. INTRODUCTION

Iron-based superconductors show rich phase diagrams, with the high-temperature superconducting dome being in the close proximity to an antiferromagnetic striped phase¹ that sets in at a temperature T_m . In addition, a structural phase transition at T_s , from the high-temperature tetragonal phase into an orthorhombic phase, has been shown to closely follow the magnetic transition²⁻⁵, i.e.: $T_s \geq T_m$. It was proposed that spin-fluctuations, associated with the striped phase, lead to emergent electronic nematic degrees of freedom at higher temperatures.^{3,6-9} These electronic nematic degrees of freedom then couple to the lattice and induce the structural phase transition to the orthorhombic phase.¹⁰⁻¹²

There is a mounting evidence for an electronic nematic state: resistivity-anisotropy measurements^{13,14} and the measurement of the elastoresistance,¹⁵ the observed anisotropies in thermopower,¹⁶ optical conductivity,^{17,18} torque magnetometry,⁵ and in STM measurements.¹⁹ Measurements of the elastic constants showed that the shear modulus strongly softens in the high temperature tetragonal phase.^{12,20-23} A theoretical analysis¹² based upon nematic fluctuations due to a strong magneto-elastic coupling showed that the inverse shear modulus is proportional to the susceptibility of the nematic order parameter χ_{nem} , which diverges at the structural phase transition, explaining its softening. The most direct evidence for the magnetic origin of nematicity so far is the scaling of the shear modulus and the NMR spin-lattice relaxation rate, seen in iron-pnictides.²⁰ An interesting open issue in this context is the lack of such scaling behavior

in iron-chalcogenides.²⁴

A relation between nematicity and the Raman response of iron based superconductors was already studied in Ref. 25 where the Kramers-Kronig transform of the Raman response was compared with the shear modulus, as well as in Ref. 26,27. Here, we demonstrate, based on an explicit microscopic theory that i) there is no enhancement of the electronic Raman response function in the B_{2g} channel upon lowering the temperature, ii) that the Raman response function develops a pronounced peak at the structural phase transition in the B_{1g} symmetry, and iii) that there is some response in the A_{1g} channel, which weakens as the temperature is lowered towards the structural transition temperature.

We start from the spin-driven scenario for the nematic phase, in which magnetic fluctuations stabilize a nematic phase, characterized by the broken C_4 symmetry. The Raman response function measures the electronic density-density correlator weighted by appropriate form factors. Since electrons interact with spin fluctuations, the latter will manifest themselves in the Raman response function in the form of corrections to the electron self energy and the Raman vertex, formally expressed in terms of Aslamazov-Larkin diagrams.²⁸ We show that the leading order Aslamazov-Larkin (AL) diagram supports only the A_{1g} and the B_{1g} symmetry, but not the B_{2g} symmetry, which explains the lack of enhancement of the Raman response signal as one approaches the structural transition in the B_{2g} channel, as seen in experiments.^{25,29} However, this leading order approach cannot account for the rapid increase in the amplitude of the Raman response function in the B_{1g} channel, as one approaches the structural transition, as seen in the experiments of Refs. 25,29. Instead it

would predict a similar increase only at the magnetic phase transition. Therefore, we go beyond the leading order approximation, and take into account collisions between spin fluctuations that become more and more important as one approaches the nematic / structural transition. Our approach is based on the exact same collisions between spin-fluctuations that led to the emergence of spin-induced nematicity in the first place. Formally this is accomplished by inserting a series of quartic paramagnon couplings, mediated by electronic excitations, into the Raman response function. Such quartic couplings contain a product of four fermionic Green's functions and give rise to a peak of the electronic Raman response function at the structural phase transition in the B_{1g} channel. On the other hand, if we re-sum such higher order AL diagrams in the A_{1g} channel, this will lead to the suppression of the Raman response in the aforementioned channel.

Here we demonstrate that the low frequency Raman response in the B_{1g} channel is given by

$$R_{B_{1g}}(\omega) = \frac{R_0(\omega)}{1 - \tilde{g} \int_q \chi_q^2}, \quad (1)$$

where ω is the frequency difference between incoming and outgoing photons and q the multi-index for momentum and frequency. $R_0(\omega)$ stands for the leading order Aslamazov-Larkin diagram, χ_q is the magnetic susceptibility, and \tilde{g} the nematic coupling constant of the theory. On the other hand, the susceptibility of the nematic order parameter of our model, in the large N limit is given by

$$\chi_{\text{nem}} = \frac{\int_q \chi_q^2}{1 - g_{\text{stat}} \int_q \chi_q^2}, \quad (2)$$

where in a purely electronic theory $\tilde{g} = g_{\text{stat}}$. In a purely electronic theory, this would then lead to the divergence of the Raman response function at the structural phase transition. However, one needs to include the effect of the lattice dynamics²¹ in order to analyze this problem. We do so by introducing nematico-elastic coupling and find that, in this case, $g_{\text{stat}} = \tilde{g} + \frac{\gamma_{\text{el}}^2}{c_s^0}$ is shifted.³⁰ Here γ_{el} is the elasto-nematic coupling constant, and c_s^0 the bare value of the orthorhombic elastic constant. We show that when magnetic and structural phase transitions are split^{2,4,5} this leads to a maximum of the amplitude of the electronic Raman response function in the B_{1g} channel at the structural phase transition, in agreement with the recent experiments.²⁹ The Raman response function could then be used to probe the dynamic excitation spectrum of the nematic degrees of freedom, similar to inelastic neutron scattering that probes the dynamic spin excitation spectrum.

The paper is organized as follows. In Sec. II we present the microscopic model for the spin-driven nematic phase. We calculate the effective action and analyze it in the large- N limit, where $N^2 - 1$ is the number of components of the collective paramagnon field. Following Ref. 7, we derive the condition for the susceptibility of the nematic order parameter to diverge. In Sec. III we then show how to calculate the Raman response function using a diagrammatic approach. We first calculate the leading order Aslamazov Larkin diagram,

and show that there is no response in the B_{2g} channel, and a finite response in the B_{1g} and the A_{1g} channels. We then calculate higher order diagrams that take into account collisions between spin-fluctuations. Finally, after summing an infinite number of these higher-order diagrams within a controlled $1/N$ expansion, we show i) that the maximum of the Raman response function in the B_{1g} channel occurs when the nematic susceptibility diverges, i.e. at the structural phase transition, and ii) that the amplitude of the Raman response function in the A_{1g} response gets suppressed. We present our conclusions in Sec. IV.

II. MICROSCOPIC MODEL: SPIN DRIVEN NEMATICITY

Two different approaches have been proposed in order to explain the origin of nematic phase in pnictides and its relation to the magnetic phase – the orbital scenario^{31–36} and the spin-driven nematic scenario.^{3,6,7} For a discussion of these approaches see for example Ref. 6. Here we follow the approach of a spin-driven nematic state. In this scenario, the nematic phase is stabilized by magnetic fluctuations that are associated with the stripe density wave (SDW) phase. The order parameter of the SDW state³⁷ can be characterized by an $O(3) \times Z_2$ manifold^{38,39} – $O(3)$ is the spin-rotational symmetry and Z_2 a discrete symmetry associated with the choice of the ordering wave-vector, $\mathbf{Q}_X = (\pi, 0)$ or $\mathbf{Q}_Y = (0, \pi)$. Let the two order parameters associated with these two ordering wave vectors be Δ_X and Δ_Y respectively. The SDW state is characterized by broken $O(3)$ and Z_2 symmetries. On the mean-field level the breaking of Z_2 and $O(3)$ symmetry occurs simultaneously. However, when one includes fluctuations, these transitions can be split. In case of joint transitions, they are usually both first order transitions.⁷ The criterion for breaking the discrete Z_2 symmetry via a second order transition is a threshold value of the magnetic correlation length ξ . Decreasing the temperature leads to an increase of ξ . Before the correlation length diverges at the magnetic phase transition temperature, the threshold value will be reached and spin-driven nematicity sets in. This naturally explains why the magnetic and structural phase boundaries are correlated and leads to an intermediate phase with Z_2 symmetry breaking without $O(3)$ symmetry breaking. This intermediate state is the nematic phase in the pnictides. It is characterized by unequal strength of the magnetic fluctuations associated with the ordering wave vectors \mathbf{Q}_X and \mathbf{Q}_Y : $\langle \Delta_X^2 - \Delta_Y^2 \rangle \neq 0$, but no long range magnetic order, $\langle \Delta_{X,Y} \rangle = 0$.

In what follows we will summarize the steps of Ref. 7 and outline the mathematical model for spin-driven nematic phase. We start from a simplified itinerant model where we include the bands near the Γ -point and the X - and Y - points in the Brillouin zone. For our main result no explicit knowledge of the detailed parametrization of the band structure is necessary, except for the fact that the band-structure is not perfectly nested. However, in order to obtain explicit numerical results we use the simplified model of Ref. 7. We consider parabolic dispersions with

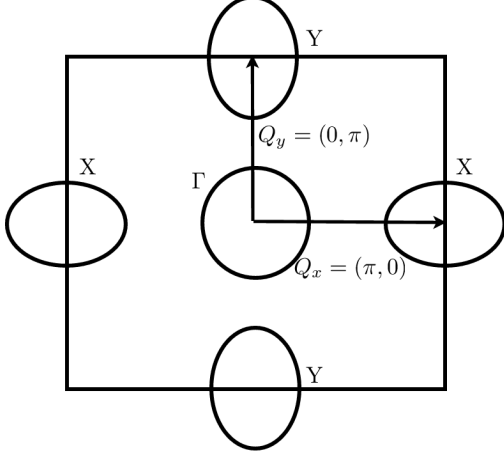


FIG. 1: Band structure: the model consists of the central hole-like Γ band, and the electron-like X and Y bands, shifted by $\mathbf{Q}_X = (\pi, 0)$ and $\mathbf{Q}_Y = (0, \pi)$, respectively.

$$\begin{aligned}
 \epsilon_{\Gamma, \mathbf{k}} &= \epsilon_0 - \frac{k^2}{2m} - \mu, \\
 \epsilon_{X, \mathbf{k} + \mathbf{Q}_X} &= -\epsilon_0 + \frac{k_x^2}{2m_x} + \frac{k_y^2}{2m_y} - \mu, \\
 \epsilon_{Y, \mathbf{k} + \mathbf{Q}_Y} &= -\epsilon_0 + \frac{k_x^2}{2m_x} + \frac{k_y^2}{2m_y} - \mu,
 \end{aligned} \quad (3)$$

where m_i are the band masses, ϵ_0 is the offset energy, and μ denotes the chemical potential. The corresponding Fermi surfaces are shown in Fig.1.

In order to study the established stripe magnetic phase, we consider the Hamiltonian that contains the interactions in the spin channel with momenta near \mathbf{Q}_X and \mathbf{Q}_Y :

$$\begin{aligned}
 \mathcal{H} &= \mathcal{H}_0 + \mathcal{H}_{\text{int}}, \\
 \mathcal{H}_0 &= \sum_{i, \mathbf{k}} \epsilon_{i, \mathbf{k}} c_{i, \mathbf{k}\alpha}^\dagger c_{i, \mathbf{k}\alpha}, \\
 \mathcal{H}_{\text{int}} &= -\frac{1}{2} u_s \sum_{i, \mathbf{q}} \mathbf{s}_{i, \mathbf{q}} \cdot \mathbf{s}_{i, -\mathbf{q}}.
 \end{aligned} \quad (4)$$

Here, $c_{i, \mathbf{k}\alpha}^\dagger$ is the creation operator of an electron with momentum \mathbf{k} , spin α and in the band i . The spin operator is given by

$$\mathbf{s}_{i, \mathbf{q}} = \sum_{\mathbf{k}} c_{\Gamma, \mathbf{k} + \mathbf{q}\alpha}^\dagger \boldsymbol{\lambda}_{\alpha\beta} c_{i, \mathbf{k}\beta}, \quad (5)$$

where $\boldsymbol{\lambda}_{\alpha\beta}$ denotes the $N^2 - 1$ component vector of the generators of the $SU(N)$ algebra. In the case $N = 2$ it holds $\boldsymbol{\lambda}_{\alpha\beta} = \frac{1}{2} \boldsymbol{\sigma}_{\alpha\beta}$ with vector of the Pauli matrixes $\boldsymbol{\sigma}$. u_s is the coupling in the spin channel, which can be expressed in terms of density-density and pair-hopping interactions between hole and electron pockets.⁴⁰

The partition function is given by

$$Z = \int dc_{i, \mathbf{k}} d c_{i, \mathbf{k}}^\dagger e^{-\beta \mathcal{H}}, \quad (6)$$

where $\beta = T^{-1}$ is the inverse temperature. Since, the interaction Hamiltonian is quadratic in the fermionic spin $\mathbf{s}_{i, \mathbf{q}}$, we can decouple it using a Hubbard-Stratonovich decoupling in the spin-channel. This way, we eliminate the quartic interaction between fermions at the expense of a functional integral over two additional bosonic fields $\boldsymbol{\Delta}_X$ and $\boldsymbol{\Delta}_Y$, with $N^2 - 1$ components. The bosonic fields couple linearly to the corresponding fermionic spin densities. After introducing the spinor

$$\Psi_{\mathbf{k}}^\dagger = \left(c_{\Gamma, \mathbf{k}\alpha}^\dagger \quad c_{X, \mathbf{k}\alpha}^\dagger \quad c_{Y, \mathbf{k}\alpha}^\dagger \right), \quad (7)$$

where α denotes every possible value of the $SU(N)$ spin index, we can write the partition function as:

$$Z = \int d\Delta_i d\Psi e^{-S[\Psi, \Delta_i]}, \quad (8)$$

with the action:

$$S[\Psi, \Delta_i] = - \int_{\mathbf{k}} \Psi_{\mathbf{k}}^\dagger \mathcal{G}_{\Delta, \mathbf{k}}^{-1} \Psi_{\mathbf{k}} + \frac{2}{u_s} \int_x (\boldsymbol{\Delta}_X^2 + \boldsymbol{\Delta}_Y^2). \quad (9)$$

Here, the matrix of the inverse Green's function \mathcal{G}_k^{-1} is given by:

$$\mathcal{G}_{\Delta, \mathbf{k}}^{-1} = \mathcal{G}_{0, \mathbf{k}}^{-1} - \mathcal{V}_\Delta, \quad (10)$$

with the bare term:

$$\mathcal{G}_{0, \mathbf{k}} = \begin{pmatrix} \hat{G}_{\Gamma, \mathbf{k}} & 0 & 0 \\ 0 & \hat{G}_{X, \mathbf{k}} & 0 \\ 0 & 0 & \hat{G}_{Y, \mathbf{k}} \end{pmatrix}, \quad (11)$$

and the interacting term:

$$\mathcal{V}_\Delta = \begin{pmatrix} 0 & -\boldsymbol{\Delta}_X \cdot \boldsymbol{\lambda} & -\boldsymbol{\Delta}_Y \cdot \boldsymbol{\lambda} \\ -\boldsymbol{\Delta}_X \cdot \boldsymbol{\lambda} & 0 & 0 \\ -\boldsymbol{\Delta}_Y \cdot \boldsymbol{\lambda} & 0 & 0 \end{pmatrix}. \quad (12)$$

$\hat{G}_{i, \mathbf{k}} = G_{i, \mathbf{k}} \hat{1}$ with $G_{i, \mathbf{k}}^{-1} = i\omega_n - \epsilon_{i, \mathbf{k}}$ and $N \times N$ unit matrix $\hat{1}$. We invert the matrix equation (10) by expanding the geometric series and obtain the following expression for \mathcal{G}_Δ that we will use later-on:

$$\mathcal{G}_\Delta = \sum_{n=0}^{\infty} (\mathcal{G}_0 \mathcal{V}_\Delta)^n \mathcal{G}_0. \quad (13)$$

A. Effective action in the large- N expansion

In this section, we first show how to obtain the Ginzburg-Landau expansion of the effective action in powers of the spin fluctuation fields $\boldsymbol{\Delta}_{X, Y}$ in the limit of large N , in the spirit similar to that of Ref. 7 where only $N = 2$ was considered.

Next, we re-formulate this effective action in terms of the collective nematic Ising variable ϕ , and analyze the equation of state for ϕ . We deduce the condition for the onset of the nematic phase by examining the susceptibility of the nematic order parameter. We begin by integrating out the fermionic degrees of freedom from Eq. (8). It follows:

$$Z = \int d\Delta_i e^{-S_{\text{eff}}[\Delta_X, \Delta_Y]} \quad (14)$$

with action:

$$S_{\text{eff}}[\Delta_X, \Delta_Y] = -\text{Tr} \ln(1 - \mathcal{G}_0 \mathcal{V}_\Delta) + \frac{2}{u_s} \int_x (\Delta_X + \Delta_Y^2). \quad (15)$$

Here, $\text{Tr}(\dots)$ refers to sum over momentum, frequency, spin, and band indices. We further expand in powers of $\Delta_{X,Y}$ to obtain:

$$S_{\text{eff}}[\Delta_X, \Delta_Y] = \frac{1}{2} \text{Tr}(\mathcal{G}_{0,k} \mathcal{V}_\Delta)^2 + \frac{1}{4} \text{Tr}(\mathcal{G}_{0,k} \mathcal{V}_\Delta)^4 + \frac{2}{u_s} \int_x (\Delta_X^2 + \Delta_Y^2). \quad (16)$$

After using a series of identities for the generators of the $SU(N)$ algebra, needed to evaluate the above traces (for details see A 2), we arrive at the following effective action in the large N limit:

$$S_{\text{eff}}[\Delta_X, \Delta_Y] = \sum_i r_{0,i} \Delta_i^2 + \sum_{i,j} u_{ij} \Delta_i^2 \Delta_j^2, \quad (17)$$

with the coefficients:

$$r_{0,i} = \frac{2}{u_s} + \frac{1}{2} \int_k G_{\Gamma,k} G_{i,k},$$

$$u_{ij} = \frac{1}{8N} \int_k G_{\Gamma,k}^2 G_{i,k} G_{j,k}. \quad (18)$$

We used the notation $\int_k = T \sum_n \int \frac{d^d k}{(2\pi)^d}$. The index $k = (\mathbf{k}, \omega_n)$ combines the momentum \mathbf{k} and the Matsubara frequency $\omega_n = (2n+1)\pi T$.

Using the identities

$$\int_k G_{\Gamma,k} G_{X,k} = \int_k G_{\Gamma,k} G_{Y,k},$$

$$\int_k G_{\Gamma,k}^2 G_{X,k}^2 = \int_k G_{\Gamma,k}^2 G_{Y,k}^2, \quad (19)$$

valid because the underlying Hamiltonian obeys the full C_4 symmetry, we can write the action in the more convenient form:

$$S_{\text{eff}}[\Delta_X, \Delta_Y] = r_0 (\Delta_X^2 + \Delta_Y^2) + \frac{u}{2} (\Delta_X^2 + \Delta_Y^2)^2 - \frac{g}{2} (\Delta_X^2 - \Delta_Y^2)^2, \quad (20)$$

with coefficients

$$r_0 = \frac{2}{u_s} + \frac{1}{2} \int_k G_{X,k} G_{\Gamma,k},$$

$$u = \frac{1}{16N} \int_k G_{\Gamma,k}^2 (G_{X,k} + G_{Y,k})^2,$$

$$g = -\frac{1}{16N} \int_k G_{\Gamma,k}^2 (G_{X,k} - G_{Y,k})^2. \quad (21)$$

r_0 , u and g have been calculated as a function of temperature and band parameters in Ref. 7. It was found that $u > 0$ and $u > g$ in general. The coupling g vanishes for circular electron pockets, but is positive for a non-zero ellipticity.

B. Nematic susceptibility in the large- N expansion

In order to investigate the possibility of the nematic transition occurring before the magnetic transition, we follow the steps of Ref. 7, and introduce two auxiliary Hubbard-Stratonovich scalar fields ϕ and ψ to decouple the quartic terms in the action (20); $\phi \rightarrow \Delta_X^2 - \Delta_Y^2$ and $\psi \rightarrow \Delta_X^2 + \Delta_Y^2$. The resulting effective action is given by

$$S_{\text{eff}} = \int_q \chi_q^{-1} (\Delta_X^2 + \Delta_Y^2) + \int_x \left(\frac{\phi^2}{2g} - \frac{\psi^2}{2u} \right) + \int_x \psi (\Delta_X^2 + \Delta_Y^2) + \int_x (\phi + h_n) (\Delta_X^2 - \Delta_Y^2), \quad (22)$$

and we have added a field h_n conjugate to the nematic order parameter $\Delta_X^2 - \Delta_Y^2$. This term is needed in order to calculate the susceptibility of the nematic order parameter. A finite value of ϕ implies non-zero expectation value of $\frac{\phi}{g} = \langle \Delta_X^2 - \Delta_Y^2 \rangle \neq 0$ and the system develops nematic order. The large- N mean field value of ψ is always non-zero and describes the strength of magnetic fluctuations. In case of split magnetic and structural phase transitions, there is no magnetic order right below the structural transition temperature, i.e. $\langle \Delta_{X,Y} \rangle = 0$. Next we integrate out the $N^2 - 1$ component fields $\Delta_{X,Y}$. If we further rescale the coupling constants to $\tilde{g} = g(N^2 - 1)$ and $\tilde{u} = u(N^2 - 1)$, required to reach a sensible large- N limit, the effective action can be written as

$$S_{\text{eff}}[\psi, \phi] = N^2 \int_q \left\{ \frac{\phi^2}{2\tilde{g}} - \frac{\psi^2}{2\tilde{u}} \right\} + \frac{N^2}{2} \int_q \left\{ \log \left[(\chi_q^{-1} + \psi)^2 - (\phi + h_n)^2 \right] \right\}. \quad (23)$$

We note that the effective action (23) has an overall pre-factor N^2 . For $N \gg 1$ the integral over the fields ϕ and ψ can be performed via the saddle-point method, i.e. by analyzing the extremum of the action. After solving for $\partial S_{\text{eff}}[\phi, \psi] / \partial \phi = \partial S_{\text{eff}}[\phi, \psi] / \partial \psi = 0$, we obtain the equations of state for ϕ

and ψ :

$$\begin{aligned}\frac{\psi}{\tilde{u}} &= \int_q \frac{\chi_q^{-1} + \psi}{(\chi_q^{-1} + \psi)^2 - (\phi + h_n)^2}, \\ \frac{\phi}{\tilde{g}} &= \int_q \frac{\phi + h_n}{(\chi_q^{-1} + \psi)^2 - (\phi + h_n)^2}.\end{aligned}\quad (24)$$

By differentiating the second equation in (24) with respect to the conjugate field, we find that, for small ϕ

$$\left. \frac{\partial \phi}{\partial h_n} \right|_{h_n=0} = \frac{\tilde{g} \int_k \chi_k^2}{1 - \tilde{g} \int_k \chi_k^2}, \quad (25)$$

where, from now on, we have shifted $\chi_k^{-1} \rightarrow \chi_k^{-1} + \psi$, which simply corresponds to the re-normalisation of the mass term due to fluctuations. Similarly to the result of Ref. 41, we find that the electronic contribution to the susceptibility of the nematic order parameter $\Delta_X^2 - \Delta_Y^2$ is given by

$$\chi_{\text{nem}}^{\text{el}} = \frac{\int_k \chi_k^2}{1 - \tilde{g} \int_k \chi_k^2}, \quad (26)$$

where χ_q^{-1} is the inverse magnetic susceptibility, and

$$\tilde{g} = -\frac{N}{16} \int_k G_{\Gamma,k}^2 (G_{X,k} - G_{Y,k})^2 \quad (27)$$

is the nematic coupling constant of the theory. In Ref. 7 it was found that for the classical phase transition in $d = 2$ and $u/g > 2$ the nematic transition pre-empt the magnetic transition, i.e. the transition lines are split. Also, the nematic transition was found to be of second order. This is the regime we are interested in. What we have calculated so far is the purely electronic contribution to the nematic susceptibility. One, however needs to include the effect of the lattice, as was pointed out in Ref. 21,30. The nematic-elastic coupling is given by the following Hamiltonian

$$\mathcal{H}_{\text{nem}} = \gamma_{\text{el}} \int dr \phi(r) (\partial_x u_x - \partial_y u_y), \quad (28)$$

where γ_{el} is the nematic-elastic coupling constant and $\mathbf{u} = (u_x, u_y)$ the phonon displacement field. The phonons renormalize the nematic coupling constant to a frequency and momentum dependent coupling

$$\tilde{g}(q, \omega) = \tilde{g} + \gamma_{\text{el}}^2 \frac{q^2}{c_s^0 q^2 - \omega^2}, \quad (29)$$

where c_s^0 is the elastic constant and q the momentum along the soft directions. In particular, if one wants to determine the location of the nematic phase transition, which is dictated by the condition of divergent nematic susceptibility, one needs to look at the static limit of the coupling constant, i.e. the limit where ω is set to zero. This leads to $g_{\text{stat}} = \tilde{g} + \frac{\gamma_{\text{el}}^2}{c_s^0}$. The full nematic susceptibility, including the effect of the coupling to the lattice, in the large N expansion is therefore given by

$$\chi_{\text{nem}} = \frac{\int_k \chi_k^2}{1 - g_{\text{stat}} \int_k \chi_k^2}, \quad (30)$$

where

$$g_{\text{stat}} = \tilde{g} + \frac{\gamma_{\text{el}}^2}{c_s^0}. \quad (31)$$

III. RAMAN RESPONSE FUNCTION

Raman scattering is a valuable tool to study strongly correlated electronic systems⁴², since it probes lattice, spin and electronic degrees of freedom. It has been used to extract information about the momentum structure and symmetry of the excitations in the cuprates^{28,43-45} and pnictides. The differential photon scattering cross section in Raman spectroscopy is directly proportional to the structure factor S :

$$S_q = -\frac{1}{\pi} [1 + n(\omega)] \text{Im} R_q, \quad (32)$$

which is related to the imaginary part to the Raman response function R through the fluctuation-dissipation theorem.⁴⁶ Here, $n(\omega)$ is the Bose-Einstein distribution function, and $q = (\mathbf{q}, \omega)$. Since the momentum of light is much smaller than the typical lattice momentum, one normally replaces $\mathbf{q} \approx 0$ in Eq. (32).

The Raman response functions measures correlations between ‘‘effective charge density’’ fluctuations $\tilde{\rho}$,

$$R(\omega) = \int_0^{1/T} d\tau e^{-i\omega\tau} \langle \tilde{\rho}(\tau) \tilde{\rho}(0) \rangle. \quad (33)$$

The effective density, weighted by the form factors that can be changed via the geometry of the photon polarization, is defined as

$$\tilde{\rho}_k = \sum_{i,k',\sigma} \gamma_{\mathbf{k}'} c_{i,k+k',\sigma}^\dagger c_{i,k',\sigma}. \quad (34)$$

σ is the spin index, i the band index, and the operator $c_{i,k,\sigma}^\dagger$ creates an electron with spin σ and momentum \mathbf{k} in band i , where $i = X, Y, \Gamma$. The function $\gamma_{\mathbf{k}}$ is related to the incident and scattered photon polarization vectors and depends on the curvature of the bands.⁴⁶ Here, we will consider the intra-orbital contributions to γ_k only, as this is the dominant process. The multi-orbital nature of different bands has been pointed out in Ref. 47.

In order to determine the Raman response function, we couple an external source field to the weighted densities and introduce the generating functional W_h according to:

$$\begin{aligned}W_h &= \frac{1}{Z} \int d\Delta_i d\Psi e^{-S[\Psi, \Delta_i] - \Psi^\dagger \mathcal{V}_h \Psi}, \\ Z &= \int d\Delta_i d\Psi e^{-S[\Psi, \Delta_i]},\end{aligned}\quad (35)$$

where $S[\Psi, \Delta_i]$ is given in Eq. (9). The elements of the matrix \mathcal{V}_h in momentum/frequency, spin and band space are

$$\mathcal{V}_{h,k_1 k_2 \sigma \sigma' i j} = h_{k_1 - k_2} \gamma_{\mathbf{k}_1} \delta_{\sigma \sigma'} \delta_{i j}, \quad (36)$$

with h being the field conjugate to the effective density. The Raman response function (33) is obtained by differentiating the generating functional W_h (35) with respect to the conjugate field h :

$$R_q = \left. \frac{\delta^2 W_h}{\delta h_q \delta h_{-q}} \right|_{h=0}. \quad (37)$$

Due to the single particle character of the source term, the generating functional Eq. (35) can be written in the form

$$\begin{aligned} W_h &= \frac{1}{Z} \int d\Delta_i d\Psi e^{\int \Psi^\dagger \mathcal{G}_{\Delta,h}^{-1} \Psi - \frac{2}{u_s} \int_x (\Delta_X^2 + \Delta_Y^2)} \\ \mathcal{G}_{\Delta,h}^{-1} &= \mathcal{G}_0^{-1} - \mathcal{V}_\Delta - \mathcal{V}_h. \end{aligned} \quad (38)$$

Since W_h contains the action that is quadratic in fermions, we integrate out the fermions and obtain:

$$\begin{aligned} W_h &= \frac{1}{Z} \int d\Delta_i e^{-S_h[\Delta_i]}, \\ S_h[\Delta_i] &= \frac{2}{u_s} \int_x (\Delta_X^2 + \Delta_Y^2) - \text{Tr} \ln \left(\mathcal{G}_{\Delta,h}^{-1} \right). \end{aligned} \quad (39)$$

We further expand:

$$\text{Tr} \ln \left(\mathcal{G}_{\Delta,h}^{-1} \right) = \text{Tr} \ln \left(\mathcal{G}_\Delta^{-1} \right) - \sum_{n=1}^{\infty} \frac{\text{Tr} \left(\mathcal{G}_\Delta \mathcal{V}_h \right)^n}{n}. \quad (40)$$

Then, using (39) and (37),

$$\begin{aligned} R_q &= \frac{1}{Z} \int d\Delta_i e^{-S_{\text{eff}}[\Delta_X, \Delta_Y]} \\ &\quad \left. \frac{\delta^2}{\delta h_q \delta h_{-q}} \exp \left[-\text{Tr} \left(\mathcal{G}_\Delta \mathcal{V}_h \right) - \frac{1}{2} \text{Tr} \left(\mathcal{G}_\Delta \mathcal{V}_h \right)^2 \right] \right|_{h=0}. \end{aligned} \quad (41)$$

Here $S_{\text{eff}}[\Delta_X, \Delta_Y] = S_h[\Delta_i]|_{h=0}$ is the effective action given by (16). We define the matrix

$$\Gamma^q = \frac{\delta \mathcal{V}_h}{\delta h_q}. \quad (42)$$

A. Self-energy and vertex correction diagrams

Next, we analyse the leading order contributions to the Raman response function. These arise from the self-energy and vertex correction diagrams depicted in Fig. 2. Both of these diagrams arise from differentiating the second term in the exponential (41) twice with respect to h

$$R_q^{V,S} = \frac{1}{Z} \int d\Delta_i e^{-S_{\text{eff}}[\Delta_X, \Delta_Y]} \text{Tr} \left[\left(\mathcal{G}_\Delta \Gamma \right)^2 \right], \quad (43)$$

and we replace $S_{\text{eff}} \rightarrow S_0$, where S_0 is the quadratic action given by

$$S_0[\Delta_i] = \frac{2}{u_s} \int (\Delta_X^2 + \Delta_Y^2) + \frac{1}{2} \text{Tr} \left(\mathcal{G}_0 \mathcal{V}_\Delta \right)^2. \quad (44)$$

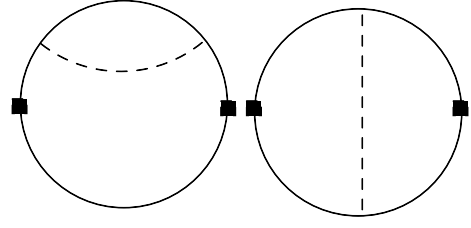


FIG. 2: Left: Contribution to the Raman response function that contains the self-energy correction to the fermionic propagator. Right: A diagram that contains a vertex renormalization correction.

In order to get the vertex correction, we replace both \mathcal{G}_Δ in (43) by $\mathcal{G}_\Delta \rightarrow \mathcal{G}_0 \mathcal{V}_\Delta \mathcal{G}_0$, which comes from the perturbative expansion of Eq. (13):

$$R_q^V = \frac{1}{Z} \int d\Delta_i e^{-S_0[\Delta_X, \Delta_Y]} \text{Tr} \left[\left(\mathcal{G}_0 \mathcal{V}_\Delta \mathcal{G}_0 \Gamma \right)^2 \right]. \quad (45)$$

In order to get the self-energy correction, we replace one of \mathcal{G}_Δ in (43) by $\mathcal{G}_\Delta \rightarrow \mathcal{G}_0$, and the other one by $\mathcal{G}_\Delta \rightarrow \left(\mathcal{G}_0 \mathcal{V}_\Delta \right)^2 \mathcal{G}_0$ to get

$$R_q^S = \frac{2}{Z} \int d\Delta_i e^{-S_0[\Delta_X, \Delta_Y]} \text{Tr} \left[\mathcal{G}_0 \Gamma \left(\mathcal{G}_0 \mathcal{V}_\Delta \right)^2 \mathcal{G}_0 \Gamma \right]. \quad (46)$$

Due to the integral over the square of the $\gamma_{\mathbf{k}}$ factor, the self-energy and vertex corrections occur in all symmetry channels. If one evaluates the sum $R^S + R^V$ explicitly, in the hot-spot approximation, one finds that there are partial cancellation in the A_{1g} and in the B_{1g} channels, and no cancellations in the B_{2g} channel. One can easily show that in $d = 2$

$$R^S + R^V \propto \int_{\mathbf{q}} \frac{1}{r_0 + q^2} \propto \log \xi, \quad (47)$$

where we have used $r_0 = \xi^{-2}$, where ξ is the magnetic correlation length.

B. Leading order Aslamazov-Larkin diagrams

The Aslamazov-Larkin contribution to the Raman response function, analyzed in Ref. 28 arises from differentiating the first term inside the exponential in (41) twice, and from replacing $\mathcal{G}_\Delta \rightarrow \left(\mathcal{G}_0 \mathcal{V}_\Delta \right)^2 \mathcal{G}_0$, which comes from the perturbative expansion of Eq. (13):

$$R_q = \frac{1}{Z} \int d\Delta_i e^{-S_{\text{eff}}[\Delta_X, \Delta_Y]} \left[\text{Tr} \left(\left(\mathcal{G}_0 \mathcal{V}_\Delta \right)^2 \mathcal{G}_0 \Gamma \right) \right]^2. \quad (48)$$

Here $S_{\text{eff}}[\Delta_X, \Delta_Y] = S_h[\Delta_i]|_{h=0}$ is the effective action given by (16).

As we will see below, the key assumption of a description based on the Aslamazov-Larkin diagrams is that one neglects the interactions between spin fluctuations. In other words, one

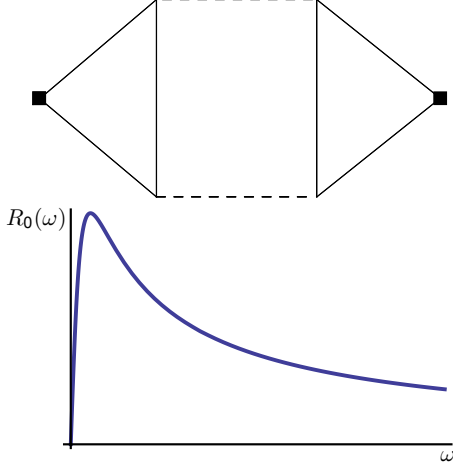


FIG. 3: Leading order Aslamazov-Larkin diagram. Raman vertices are denoted by black squares. Imaginary part of the Raman response function as a function of frequency $\text{Im}R_0(\omega)$, in $d = 2$.

approximates the effective action in (48) by quadratic action Eq. (44). While this assumption is frequently justified, it is not allowed in the theory of spin-driven nematicity, as we will show later.

The leading order Aslamazov-Larkin diagram, depicted in Fig. 3 can be calculated as

$$R_0(\omega) = T \sum_{i=X,Y,n} \int_{\mathbf{q}} \Lambda_i^2(\mathbf{q}, \Omega_n, \omega) \chi(\mathbf{q}, \Omega_n) \chi(\mathbf{q}, \Omega_n - \omega) \quad (49)$$

with

$$\begin{aligned} \Lambda_i(\mathbf{q}, \Omega, \omega) &= \Lambda_i^{(1)}(\mathbf{q}, \Omega, \omega) + \Lambda_i^{(2)}(-\mathbf{q}, -\Omega, -\omega), \\ \Lambda_i^{(1)}(\mathbf{q}, \Omega, \omega) &= T \sum_n \int_{\mathbf{k}} \gamma_{\mathbf{k}} G_{\Gamma}(\mathbf{k}, \nu_n - \omega) G_{\Gamma}(\mathbf{k}, \nu_n) \\ &\quad \times G_i(\mathbf{k} - \mathbf{q}, \nu_n - \Omega), \\ \Lambda_i^{(2)}(\mathbf{q}, \Omega, \omega) &= T \sum_n \int_{\mathbf{k}} \gamma_{\mathbf{k}} G_i(\mathbf{k}, \nu_n - \omega) G_i(\mathbf{k}, \nu_n) \\ &\quad \times G_{\Gamma}(\mathbf{k} - \mathbf{q}, \nu_n - \Omega), \end{aligned} \quad (50)$$

similar to what was found in Ref. 48.

1. Raman response in different symmetry channels

In the concept of the pairing symmetry in high-temperature superconductors successful theoretical models supported by experiments have been developed in order to explain the symmetry sensitivity of the Raman response function.⁴⁹ Similarly, here, before we explicitly evaluate the leading order Aslamazov-Larkin diagram, we analyze the contribution to it in the various symmetry channels. Higher order corrections that will be discussed later do not alter this symmetry-based analysis. We show that the Aslamazov-Larkin diagram, given

by Eq. (49) and (50), only supports the B_{1g} and the A_{1g} symmetry channels. Let us consider the structure of the terms in (49) which arise from

$$R_0^{(11)}(\omega) := T \sum_{i=X,Y,n} \int_{\mathbf{q}} \left[\Lambda_i^{(1)}(\mathbf{q}, \Omega_n, \omega) \right]^2 \times \chi(\mathbf{q}, \Omega_n) \chi(\mathbf{q}, \Omega_n - \omega). \quad (51)$$

The term (51) can be re-written in the following form

$$\begin{aligned} R_0^{(11)}(\omega) &= \frac{T}{2} \sum_n \int_{\mathbf{q}} \int_{\mathbf{k}} \int_{\mathbf{p}} \gamma_{\mathbf{k}} \gamma_{\mathbf{p}} \chi(\mathbf{q}, \Omega_n) \chi(\mathbf{q}, \Omega_n - \omega) \\ &\quad \times (E_{A_{1g}}(\omega, \Omega_n, \mathbf{k}, \mathbf{q}) E_{A_{1g}}(\omega, \Omega_n, \mathbf{p}, \mathbf{q}) \\ &\quad + E_{B_{1g}}(\omega, \Omega_n, \mathbf{k}, \mathbf{q}) E_{B_{1g}}(\omega, \Omega_n, \mathbf{p}, \mathbf{q})), \end{aligned} \quad (52)$$

where we have classified the appropriate combinations of Green's functions according to their symmetry into

$$\begin{aligned} E_{A_{1g}}(\omega, \Omega_n, \mathbf{k}, \mathbf{q}) &= T \sum_m G_{\Gamma}(\mathbf{k}, \nu_m - \omega) G_{\Gamma}(\mathbf{k}, \nu_m) \\ &\quad \times G^{(+)}(\mathbf{k} - \mathbf{q}, \nu_m - \Omega_n), \\ E_{B_{1g}}(\omega, \Omega_n, \mathbf{k}, \mathbf{q}) &= T \sum_m G_{\Gamma}(\mathbf{k}, \nu_m - \omega) G_{\Gamma}(\mathbf{k}, \nu_m) \\ &\quad \times G^{(-)}(\mathbf{k} - \mathbf{q}, \nu_m - \Omega_n), \end{aligned} \quad (53)$$

and we have defined $G^{(\pm)} = G_X \pm G_Y$. From Eq. (53), we see that the response will be non-zero only for γ factors in the A_{1g} or the B_{1g} symmetry. Similarly, using the same line of arguments, one can show that all other terms in (49) support the A_{1g} or the B_{1g} symmetry only. We have thus ruled out the response in the B_{2g} channel.

2. Explicit calculation of the leading order Aslamazov-Larkin diagram

The leading order Aslamazov-Larkin diagram has been evaluated in Ref. 28, assuming that the main contribution comes from the hot-spot regions and that the momenta of the fluctuations are peaked around $\mathbf{q} \approx \mathbf{Q}_{X,Y}$. After the analytic continuation to the real frequencies, we found that the imaginary part of the Raman response function, which is a quantity of experimental interest, is given by

$$\begin{aligned} \text{Im}R_0(\omega + i0^+) &= \int_{-\infty}^{\infty} \frac{d\epsilon}{\pi} [n(\epsilon) - n(\epsilon + \omega)] \\ &\quad \times \int_{\mathbf{q}} \text{Im} [\chi^R(\epsilon, \mathbf{q})] \text{Im} [\chi^R(\epsilon + \omega, \mathbf{q})], \end{aligned} \quad (54)$$

with the spin propagator in the tetragonal phase given by:

$$\chi^R(\mathbf{q}, \Omega) = \frac{1}{r_0 + \mathbf{q}^2 - i\Omega}, \quad (55)$$

where r_0 tunes the distance from the magnetic transition, see Eq. (21). In $d = 2$ the \mathbf{q} integral in Eq. (54) can be performed exactly, which leads to the following expression

$$\text{Im} [R_0(\omega + i0^+)]_{d=2} = \int_0^\infty d\epsilon [n(\epsilon_+) - n(\epsilon_-)] \frac{\epsilon_+ \epsilon_-}{\epsilon_+^2 - \epsilon_-^2} \times [F(\epsilon_+) - F(\epsilon_-)], \quad (56)$$

with

$$F(x) = \frac{1}{x} \left(\arctan \frac{r_0}{x} - \frac{\pi}{2} \text{sgn}(x) \right). \quad (57)$$

We defined $\epsilon_\pm = \epsilon \pm \omega/2$. The plot of the function (56) is shown in Fig. 3. In particular one can deduce that, in the regime where temperature T is the biggest scale, $T \gg r_0$, $R_0(\omega)_{d=2} \simeq \frac{\omega T}{r_0^2}$ for small frequencies ω , while the amplitude of the Raman response function scales as $R_0^{\text{max}}(\omega)_{d=2} \simeq \frac{T}{r_0}$ in this regime.

In summary, we have shown that the leading order Aslamazov-Larkin diagram gives a non-zero response in the B_{1g} and A_{1g} symmetries only. It predicts the divergence of the Raman response at the magnetic transition, and does not carry any signatures of the structural transition. We therefore need to go beyond the leading order Aslamazov-Larkin diagram.

C. Higher order Aslamazov-Larkin-like diagrams

Next, we go beyond the quadratic action approximation for S_{eff} in (48), and include the full quartic action to evaluate the Raman response function. As we will show, diagrammatically this corresponds to inserting a series of fermionic boxes that resemble the structure of the nematic coupling constant \tilde{g} into the leading order Aslamazov-Larkin diagram in the B_{1g} symmetry. These diagrams take into account the collisions between spin fluctuations which were not accounted for in the leading order Aslamazov-Larkin diagram.

First we show how these terms arise from the diagrammatic expansion. We start from Eq. (48), but this time we go beyond the quadratic approximation for the effective action, and include quartic terms

$$R_q = \frac{1}{Z} \int d\Delta_i e^{-S_{\text{eff}}[\Delta_i]} \left[\text{Tr} \left((\mathcal{G}_0 \mathcal{V}_\Delta)^2 \mathcal{G}_0 \Gamma \right) \right]^2 \quad (58)$$

where

$$S_{\text{eff}}[\Delta_i] = S_0[\Delta_i] + \frac{1}{4} \text{Tr} (\mathcal{G}_0 \mathcal{V}_\Delta)^4, \quad (59)$$

with the bare action

$$S_0[\Delta_i] = \frac{2}{u_s} \int_x (\Delta_X^2 + \Delta_Y^2) + \frac{1}{2} \text{Tr} (\mathcal{G}_0 \mathcal{V}_\Delta)^2. \quad (60)$$

We further expand the exponential

$$e^{-\frac{1}{4} \text{Tr} (\mathcal{G}_0 \mathcal{V}_\Delta)^4} \approx \sum_{m=0}^{\infty} \frac{1}{m!} \left[\frac{-1}{4} \text{Tr} (\mathcal{G}_0 \mathcal{V}_\Delta)^4 \right]^m \quad (61)$$

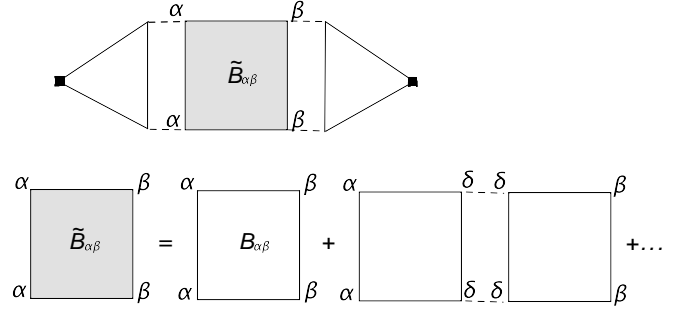


FIG. 4: Re-summed Raman response function. The resummed box $\tilde{B}_{\alpha\beta}$ is shaded grey. The first index of the matrix B denotes the type $\alpha = X, Y$ of entering spin fluctuations, and the second index the type of exiting spin fluctuations. We insert the grey shaded box into the Raman response, and make some further simplifications to evaluate the Raman response function (see the main text).

to obtain

$$R_q = \sum_{m=0}^{\infty} \frac{1}{m!} R_q^{(m)}, \quad (62)$$

where we averaged the following terms with respect to the Gaussian collective spin action:

$$R_q^{(m)} = \left\langle \left[\frac{-1}{4} \text{Tr} (\mathcal{G}_0 \mathcal{V}_\Delta)^4 \right]^m \left[\text{Tr} \left((\mathcal{G}_0 \mathcal{V}_\Delta)^2 \mathcal{G}_0 \Gamma \right) \right]^2 \right\rangle_{S_0}.$$

In order to evaluate the expectation values one performs contractions of the Δ fields. We obtain a series of diagrams that look like the leading order Aslamazov-Larkin diagram with an arbitrary number of inserted fermionic boxes, depicted in Fig. 4.

The higher order diagrams effectively take collisions between spin fluctuations into account, which have been neglected in the leading order Aslamazov-Larkin diagram. As one approaches the transition line, collisions between spin fluctuations become more and more important and one would anticipate significant changes in the Raman response function due to these processes. As we will show, the re-summation of boxed Aslamazov-Larkin diagrams will lead to the maximum of the Raman response function at the structural phase transition in the B_{1g} channel, and the suppression of the response in the A_{1g} channel.

The next task is to re-sum an infinite number of such diagrams. Every box can be characterized by two indices: the first one denotes the type of incoming spin fluctuations, this can be either X or Y and the second one denotes the type of exiting spin fluctuation. Let us denote this box $B_{\alpha\beta}$. Summing all boxed diagrams can be most efficiently expressed as:

$$\begin{aligned} R(\omega) &= R_0(\omega) + T^2 \sum_{\Omega, \Omega'} \int_{\mathbf{q}, \mathbf{q}'} \Lambda_\alpha(\omega, \Omega, \mathbf{q}) \\ &\times \chi(\mathbf{q}, \Omega) \chi(\mathbf{q}, \Omega - \omega) \\ &\times \tilde{B}_{\alpha\beta}(\mathbf{q}, \mathbf{q}', \Omega, \Omega', \omega) \chi(\mathbf{q}', \Omega') \\ &\times \chi(\mathbf{q}', \Omega' - \omega) \Lambda_\beta(\omega, \Omega', \mathbf{q}'). \end{aligned} \quad (63)$$

For our analysis it is sufficient to calculate the box $B_{\alpha\beta}$ at momenta $\mathbf{q}, \mathbf{q}' \approx \mathbf{Q}_{X,Y}$ and zero frequencies, which is justified for small incoming Raman frequency ω , and in the classical regime relevant near a finite temperature phase transition. We write the Raman response function in the tetragonal phase:

$$R(\omega) \approx R_0(\omega) + \int_{\mathbf{q}, \mathbf{q}'} \Lambda_\alpha(\omega, 0, \mathbf{q}) \tilde{B}_{\alpha\beta} \times \chi^2(\mathbf{q}, 0) \chi^2(\mathbf{q}', 0) \Lambda_\beta(\omega, 0, \mathbf{q}'), \quad (64)$$

where $R_0(\omega)$ is the leading order diagram.

The symmetry of the fermionic triangle is such that

$$\begin{aligned} \Lambda_X^{B_{1g}} &= -\Lambda_Y^{B_{1g}}, \\ \Lambda_X^{A_{1g}} &= \Lambda_Y^{A_{1g}}. \end{aligned} \quad (65)$$

This relation can be obtained by simply performing a coordinate system rotation by $\pi/2$ inside the momenta integrals in (50). This allows us to explicitly perform the matrix multiplication, which yields:

$$\begin{aligned} \tilde{R}_{B_{1g}}(\omega) &= R_0(\omega) + R_0(\omega) (\tilde{B}_{XX} - \tilde{B}_{XY}) \int_{\mathbf{q}} \chi^2(\mathbf{q}, 0), \\ \tilde{R}_{A_{1g}}(\omega) &= R_0(\omega) + R_0(\omega) (\tilde{B}_{XX} + \tilde{B}_{XY}) \int_{\mathbf{q}} \chi^2(\mathbf{q}, 0). \end{aligned} \quad (66)$$

Next we need to determine an expression for the full box $\tilde{B}_{\alpha\beta}$, i.e. perform a sum over the leading box-diagrams within the $1/N$ expansion. This is illustrated in Fig. 4 and can be written as:

$$\begin{aligned} \tilde{B}_{\alpha\beta} &= B_{\alpha\beta} + B_{\alpha\delta} B_{\delta\beta} \int_{\mathbf{q}'} \chi^2(\mathbf{q}', 0) + \dots \\ &= \sum_{m=1}^{\infty} (B^m)_{\alpha\beta} \left(\int_{\mathbf{q}} \chi^2(\mathbf{q}, 0) \right)^{m-1}, \end{aligned} \quad (67)$$

The matrix B was deduced from Eq. (63) and Eq. (B4). For details about explicit evaluation of the $SU(N)$ trace pre-factor (which arises from contractions of products of λ matrices in (12)) for boxed diagram containing arbitrary number of boxes m , please see Appendix B. The matrix B of irreducible boxes is then given as

$$B = -\frac{N}{8} \begin{pmatrix} g_{XX} & g_{XY} \\ g_{XY} & g_{XX} \end{pmatrix} \quad (68)$$

where we used the abbreviation

$$\begin{aligned} g_{XX} &= \int_k G_{\Gamma,k}^2 G_{X,k}^2, \\ g_{XY} &= \int_k G_{\Gamma,k}^2 G_{X,k} G_{Y,k}, \end{aligned} \quad (69)$$

and used that by symmetry: $\int_k G_{\Gamma,k}^2 G_{X,k}^2 = \int_k G_{\Gamma,k}^2 G_{Y,k}^2$.

The m th power of the matrix B is given by

$$B^m = \frac{1}{2} \left(\frac{-N}{8} \right)^m \begin{pmatrix} (g_+^m + g_-^m) & (g_+^m - g_-^m) \\ (g_+^m - g_-^m) & (g_+^m + g_-^m) \end{pmatrix}, \quad (70)$$

where $g_{\pm} = g_{XX} \pm g_{XY}$. From this analysis follows that

$$\begin{aligned} \tilde{R}_{B_{1g}}(\omega) &= R_0(\omega) \sum_{m=0}^{\infty} \left(\frac{-Ng_-}{8} \right)^m \left(\int_{\mathbf{q}} \chi^2(\mathbf{q}, 0) \right)^m \\ &= R_0(\omega) + R_0(\omega) \frac{\tilde{g} \int_{\mathbf{q}} \chi^2(\mathbf{q}, 0)}{1 - \tilde{g} \int_{\mathbf{q}} \chi^2(\mathbf{q}, 0)}, \\ \tilde{R}_{A_{1g}}(\omega) &= R_0(\omega) \sum_{m=0}^{\infty} \left(\frac{-Ng_+}{8} \right)^m \left(\int_{\mathbf{q}} \chi^2(\mathbf{q}, 0) \right)^m \\ &= R_0(\omega) + R_0(\omega) \frac{\tilde{u} \int_{\mathbf{q}} \chi^2(\mathbf{q}, 0)}{1 + \tilde{u} \int_{\mathbf{q}} \chi^2(\mathbf{q}, 0)}, \end{aligned} \quad (71)$$

where

$$\tilde{g} = -\frac{N}{16} \int_k G_{\Gamma,k}^2 (G_{X,k} - G_{Y,k})^2 \quad (72)$$

is precisely the nematic coupling constant of Eq. (21) for the effective action, and \tilde{u} is the other quartic term in Eq. (21), with $\tilde{u} > 0$, as found in Ref 7. From (71), we see that the Raman response in the A_{1g} channel gets suppressed, due to the term in the denominator, which grows as one approaches the transition. On the other hand, in the B_{1g} channel, after performing the analytic continuation to real frequencies and taking the imaginary part, we get that

$$\text{Im} \tilde{R}_{B_{1g}}(\omega) = \text{Im} [R_0(\omega)] (1 + \tilde{g} \chi_{\text{nem}}^{\text{el}}), \quad (73)$$

where

$$\chi_{\text{nem}}^{\text{el}} = \frac{\int_{\mathbf{q}} \chi^2(\mathbf{q}, 0)}{1 - \tilde{g} \int_{\mathbf{q}} \chi^2(\mathbf{q}, 0)} \quad (74)$$

is the electronic contribution to the nematic susceptibility calculated in the large N limit¹² for the model described in Sec. II A. As was pointed out in Ref. 30, the enhancement of the static nematic coupling constant (31) does not enter the Raman response, due to the fact that the Raman response operates in the dynamical limit ($\mathbf{q} = 0$ and finite ω), and the static and dynamic limits do not commute³⁰. At the nematic / structural phase transition the nematic susceptibility (30) diverges, and

$$\left(\tilde{g} + \frac{\gamma_{\text{el}}^2}{c_0^2} \right) \int_{\mathbf{q}} \chi_{\mathbf{q}}^2 = 1. \quad (75)$$

Consequently the Raman response function in the B_{1g} channel, given by (73), has a maximum rather than a divergence at the structural phase transition.

IV. CONCLUSION

In summary, we have shown that the Raman scattering can be used as a tool to probe the nematic phase in pnictides. We have presented a calculation that demonstrates that, in the low-frequency limit, and large N limit, the Raman response function shows a clear maximum at the structural transition temperature in the B_{1g} channel.

In our model, the electronic nematic phase in pnictides is stabilized by spin-fluctuations associated with the striped phase, and occurs as a thin sliver above the magnetic transition temperature. In order to calculate the Raman response function, we have gone beyond the leading order Aslamazov-Larkin diagram, and included higher order diagrams that contain a series of quartic paramagnon couplings, mediated by electronic excitations. Such quartic couplings contain a product of four fermionic Green's functions and include the effect of collisions between spin fluctuations. When re-summed these diagrams lead to the maximum of the electronic Raman response function at the structural transition in the B_{1g} channel, and the suppression of the response in the A_{1g} channel.

The method that we developed analysed the Raman response function only in the regime of small frequencies. It would be desirable to extend it to the entire frequency range, such that one can analyse the entire shape of the Raman response function as a function of temperature, and possibly be able to extract some information about the dynamical nematic susceptibility.

Further, one might expect a charge driven nematic phase to have similar signatures in the Raman response function. This could be relevant to the peculiar case of FeSe, where the nematic phase has been detected, but no magnetic phase has been seen.^{24,50} In order to do so, we would need to develop a theoretical method that goes beyond the large N expansion.

V. ACKNOWLEDGEMENT

We acknowledge useful discussions with A. Chubukov and R. Fernandes. U.K. acknowledges the support from the Helmholtz Association, through Helmholtz post-doctoral grant PD-075 "Unconventional order and superconductivity in pnictides". J.S., F.K., T.B. and R.H. acknowledge the support from Deutsche Forschungsgemeinschaft (DFG) through the Priority Program SPP 1458 "Hochtemperatur-Supraleitung in Eisenpniktiden" (project-nos. SCHM 1031/5-1 and HA2071/7-2). Y.G. acknowledges financial support from ANR grant PNICTIDES.

Note: In the final stages of the preparations of the manuscript we became aware of arXiv:1504.05054, where the behaviour of the Raman response function in the vicinity of the structural transition has been analyzed. Where there is overlap with this work, our results agree.

Appendix A: Effective action of the $SU(N)$ fermionic model

1. Some useful $SU(N)$ identities

Here, we present some useful identities for the structure constants of $SU(N)$. They have been used to determine the scaling of the boxed Aslamazov-Larkin diagrams with N , and to develop the Ginzburg-Landau expansion of the effective action in powers of spin fluctuation fields Δ (see Sec. II). We begin by listing some standard $SU(N)$ identities for the matrices λ_i , where $i = 1, \dots, N^2 - 1$. All repeated indices are

summed over.

$$\{\lambda_j, \lambda_k\} = \frac{1}{N} \delta_{jk} + \mathbf{d}_{jkl} \lambda_l \quad \mathbf{d}_{jkl} = \mathbf{d}_{kjl}, \quad (\text{A1})$$

$$[\lambda_j, \lambda_k] = i \mathbf{f}_{jkl} \lambda_l \quad \mathbf{f}_{jkl} = -\mathbf{f}_{kjl}, \quad (\text{A2})$$

$$\lambda_j \lambda_k = \frac{1}{2N} \delta_{jk} + \frac{1}{2} \mathbf{R}_{jkl} \lambda^l, \quad (\text{A3})$$

$$\mathbf{R}_{jkl} := \mathbf{d}_{jkl} + i \mathbf{f}_{jkl}. \quad (\text{A4})$$

Here \mathbf{d}_{jkl} is symmetric under the exchange of its indices, while \mathbf{f}_{jkl} is antisymmetric under the exchange of neighbouring indices. Further, some useful relations for the summations of structure constants can be derived,^{51,52} which read

$$\mathbf{d}_{akl} \mathbf{d}_{bkl} = \frac{N^2 - 4}{N} \delta_{ab}, \quad (\text{A5})$$

$$\mathbf{f}_{akl} \mathbf{f}_{bkl} = N \delta_{ab}, \quad (\text{A6})$$

$$\sum_i \mathbf{d}_{ijj} = 0. \quad (\text{A7})$$

Useful identities that involve the traces of the $SU(N)$ matrices are

$$\text{Tr}(\lambda_i) = 0, \quad (\text{A8})$$

$$\text{Tr}(\mathbb{1}) = N, \quad (\text{A9})$$

$$\text{Tr}(\lambda_i \lambda_j) = \frac{1}{2} \delta_{ij}. \quad (\text{A10})$$

In order to analyse the trace of the product of four $SU(N)$ generators we evaluate

$$\begin{aligned} \text{Tr}(\lambda_i \lambda_j \lambda_k \lambda_l) &= \text{Tr} \left[\left(\frac{1}{2N} \delta_{ij} + \frac{1}{2} \mathbf{R}_{ijp} \lambda_p \right) \right. \\ &\quad \times \left. \left(\frac{1}{2N} \delta_{kl} + \frac{1}{2} \mathbf{R}_{klr} \lambda_r \right) \right] \\ &= \frac{1}{4N} \delta_{ij} \delta_{kl} + \frac{1}{8} \mathbf{R}_{ijp} \mathbf{R}_{klp}, \end{aligned} \quad (\text{A11})$$

where we used the identity (A3) in the first line, as well as Eq. (A8) and Eq. (A10) in the second line. These results will be of importance for the subsequent analysis of higher order diagrams.

2. Effective action from tr log expansion

First we calculate the quadratic terms in the free energy expansion. This is given by

$$\begin{aligned} \frac{1}{2} \text{Tr}(\mathcal{G}_0 \mathcal{V}_\Delta)^2 &= \sum_\alpha \int_k G_{\alpha,k} G_{\Gamma,k} \sum_{i,j=1}^{N^2-1} \text{Tr}(\lambda_i \lambda_j) \Delta_\alpha^i \Delta_\alpha^j \\ &= \frac{1}{2} \sum_\alpha \int_k G_{\alpha,k} G_{\Gamma,k} |\Delta_\alpha|^2, \end{aligned} \quad (\text{A12})$$

where $\alpha = X, Y$ and we used the identity (A10).

Next we calculate the quartic term in the free energy expansion

$$\begin{aligned}
\frac{1}{4}\text{Tr}(\mathcal{G}_0\mathcal{V}_\Delta)^4 &= \frac{1}{2}\text{Tr}(\lambda_i\lambda_j\lambda_k\lambda_l) \\
&\times \sum_{\alpha=X,Y} g_{\alpha\alpha}\Delta_\alpha^i\Delta_\alpha^j\Delta_\alpha^k\Delta_\alpha^l \\
&+ \frac{1}{2}\text{Tr}(\lambda_i\lambda_j\lambda_k\lambda_l) \\
&\times \sum_{\alpha=X,Y} g_{\alpha\bar{\alpha}}\Delta_{\bar{\alpha}}^i\Delta_{\bar{\alpha}}^j\Delta_\alpha^k\Delta_\alpha^l,
\end{aligned} \tag{A13}$$

with

$$\begin{aligned}
g_{XX} &= g_{YY} = \int_k G_{X,k}^2 G_{\Gamma,k}^2, \\
g_{XY} &= g_{YX} = \int_k G_{X,k} G_{Y,k} G_{\Gamma,k}^2,
\end{aligned} \tag{A14}$$

and we used the notation $\bar{\alpha}$ for 'not α ', i.e. if $\alpha = X$ then $\bar{\alpha} = Y$ and vice versa. We further substitute the identity (A11) in (A13), to write

$$\frac{1}{4}\text{Tr}(G\mathcal{V}_\Delta)^4 = K_1 + K_2, \tag{A15}$$

where

$$\begin{aligned}
K_1 &= \frac{1}{8N} \sum_{\alpha=X,Y} g_{\alpha\alpha} |\Delta_\alpha|^4 \\
&+ \frac{1}{8N} \sum_{\alpha=X,Y} g_{\alpha\bar{\alpha}} |\Delta_\alpha|^2 |\Delta_{\bar{\alpha}}|^2, \\
K_2 &= \sum_{\alpha=X,Y} \frac{g_{\alpha\alpha}}{16} \mathbf{R}_{ijp} \mathbf{R}_{klp} \Delta_\alpha^i \Delta_\alpha^j \Delta_\alpha^k \Delta_\alpha^l \\
&+ \sum_{\alpha=X,Y} \frac{g_{\alpha\bar{\alpha}}}{16} \mathbf{R}_{ijp} \mathbf{R}_{klp} \Delta_{\bar{\alpha}}^i \Delta_{\bar{\alpha}}^j \Delta_\alpha^k \Delta_\alpha^l.
\end{aligned} \tag{A16}$$

Since $K_2 \sim N^{-5}$, while $K_1 \sim N^{-1}$, the term K_2 can be omitted in the large N limit.

Combining (A16) and (A12), the effective action in the large N limit can be written as

$$S_{\text{eff}}[\Delta_X, \Delta_Y] = \sum_i r_{0,i} \Delta_i^2 + \sum_{i,j} u_{ij} \Delta_i^2 \Delta_j^2, \tag{A17}$$

with the coefficients:

$$\begin{aligned}
r_{0,i} &= \frac{2}{u_s} + \frac{1}{2} \int_k G_{\Gamma,k} G_{i,k}, \\
u_{ij} &= \frac{1}{8N} \int_k G_{\Gamma,k}^2 G_{i,k} G_{j,k}.
\end{aligned} \tag{A18}$$

We note that in the large N approximation there are no $\Delta_X \cdot \Delta_Y$ terms in the action; however if one considers corrections to large N these terms might appear in the effective action.

Appendix B: Identities containing products of traces of $SU(N)$ generators

In this appendix we derive further identities for the traces of the $SU(N)$ generators, which have been used to deduce the dependence of the Aslamazov-Larkin boxed diagrams on N . In particular, we would like to calculate

$$\begin{aligned}
T_m &:= \text{Tr}(\lambda_{i_1} \lambda_{i_2}) \text{Tr}(\lambda_{i_2} \lambda_{i_1} \lambda_{i_3} \lambda_{i_4}) \\
&\times \text{Tr}(\lambda_{i_4} \lambda_{i_3} \lambda_{i_5} \lambda_{i_6}) \dots \\
&\times \text{Tr}(\lambda_{i_{2m}} \lambda_{i_{2m-1}} \lambda_{i_{2m+1}} \lambda_{i_{2m+2}}) \\
&\times \text{Tr}(\lambda_{i_{2m+2}} \lambda_{i_{2m+1}}).
\end{aligned} \tag{B1}$$

We begin by considering $m = 1$. Written out explicitly, it follows:

$$\begin{aligned}
T_1 &= \text{Tr}(\lambda_i \lambda_j) \text{Tr}(\lambda_k \lambda_l) \text{Tr}(\lambda_j \lambda_i \lambda_l \lambda_k) \\
&= \left(\frac{1}{4} \delta_{ij} \delta_{kl} \right) \left(\frac{1}{4N} \delta_{ij} \delta_{kl} + \frac{1}{8} \mathbf{R}_{jir} \mathbf{R}_{lkr} \right) \\
&= \frac{1}{4} \frac{1}{(4N)} \sum_{ijkl} \delta_{ij} \delta_{kl} + \sum_{ikr} \frac{1}{32} \mathbf{R}_{iir} \mathbf{R}_{kkr} \\
&= \frac{1}{4} \frac{1}{(4N)} (N^2 - 1)^2,
\end{aligned} \tag{B2}$$

where we have used (A10) and (A11) to get to the second line, and the fact that $\mathbf{R}_{iir} = 0$ in the penultimate line, which is a consequence of (A7) and the antisymmetry of \mathbf{f} . Using the same set of identities, we find that

$$\begin{aligned}
T_2 &= \text{Tr}(\lambda_i \lambda_j) \text{Tr}(\lambda_k \lambda_l) \text{Tr}(\lambda_j \lambda_i \lambda_s \lambda_r) \text{Tr}(\lambda_r \lambda_s \lambda_l \lambda_k) \\
&= \left(\frac{1}{4} \delta_{ij} \delta_{kl} \right) \left(\frac{1}{4N} \delta_{ij} \delta_{sr} + \frac{1}{8} \mathbf{R}_{jit} \mathbf{R}_{srt} \right) \\
&\times \left(\frac{1}{4N} \delta_{sr} \delta_{kl} + \frac{1}{8} \mathbf{R}_{rsz} \mathbf{R}_{lkz} \right) \\
&= \frac{1}{4} \left(\frac{1}{4N} \right)^2 \sum_{ijklsr} \delta_{ij} \delta_{kl} \delta_{sr} \\
&= \frac{1}{4} \left(\frac{1}{4N} \right)^2 (N^2 - 1)^3.
\end{aligned} \tag{B3}$$

Similarly, one can deduce that

$$T_m = \frac{1}{4} \left(\frac{1}{4N} \right)^m (N^2 - 1)^{m+1} \approx \frac{N^2}{4} \left(\frac{N}{4} \right)^m. \tag{B4}$$

¹ J. Paglione, and R. L. Greene, Nature Phys. **6**, 645 (2010).

² M. G. Kim, R. M. Fernandes, A. Kreyssig, J. W. Kim, A. Thaler,

S. L. Bud'ko, P. C. Canfield, R. J. McQueeney, J. Schmalian, and A. I. Goldman, Phys. Rev. B **83**, 134522 (2011).

- ³ R. M. Fernandes, and J. Schmalian, *Supercond. Sci. Technol.* **25**, 084005 (2012).
- ⁴ C. R. Rotundu, and R. J. Birgeneau, *Phys. Rev. B* **84**, 092501 (2011).
- ⁵ S. Kasahara, H. J. Shi, K. Hashimoto, S. Tonegawa, Y. Mizukami, T. Shibauchi, K. Sugimoto, T. Fukuda, T. Terashima, A. H. Nvidomskyy, and Y. Matsuda, *Nature* **486**, 382 (2012).
- ⁶ R. M. Fernandes, A. V. Chubukov, and J. Schmalian, *Nature Phys.* **10**, 97-104 (2014).
- ⁷ R. M. Fernandes, A. V. Chubukov, J. Knolle, I. Eremin, and J. Schmalian, *Phys. Rev. B* **85**, 024534 (2012).
- ⁸ C. Xu, M. Müller, and S. Sachdev, *Phys. Rev. B* **78**, 020501(R) (2008).
- ⁹ C. Fang, H. Yao, W. F. Tsai, J. P. Hu, and S. A. Kivelson, *Phys. Rev. B* **77**, 224509 (2008).
- ¹⁰ Y. Qi, and C. Xu, *Phys. Rev. B* **80**, 094402 (2009).
- ¹¹ A. Cano, M. Civelli, I. Eremin, and I. Paul, *Phys. Rev. B* **82**, 020408(R) (2010).
- ¹² R. M. Fernandes, L. H. VanBebber, S. Bhattacharya, P. Chandra, V. Keppens, D. Mandrus, M. A. McGuire, B. C. Sales, A. S. Sefat, and J. Schmalian, *Phys. Rev. Lett.* **105**, 157003 (2010).
- ¹³ M. A. Tanatar, E. C. Blomberg, A. Kreyssig, M. G. Kim, N. Ni, A. Thaler, S. L. Bud'ko, P. C. Canfield, A. I. Goldman, I. I. Mazin, and R. Prozorov, *Phys. Rev. B* **81**, 184508 (2010).
- ¹⁴ J. H. Chu, H. H. Kuo, J. G. Analytis, and I. R. Fisher, *Science* **337**, 719 (2012).
- ¹⁵ J. H. Chu, J. G. Analytis, K. De Greve, P. L. McMahon, Z. Islam, Y. Yamamoto, and I. R. Fisher, *Science* **329**, 824 (2010).
- ¹⁶ Shuai Jiang, H. S. Jeevan, Jinkui Dong, and P. Gegenwart, *Phys. Rev. Lett.* **110**, 067001 (2013).
- ¹⁷ A. Dusza, A. Lucarelli, F. Pfuner, J. H. Chu, I. R. Fisher, and L. Degiorgi, *Europhys. Lett.* **93**, 37002 (2011).
- ¹⁸ M. Nakajima, T. Liang, S. Ishida, Y. Tomioka, K. Kihou, C. H. Lee, A. Iyo, H. Eisaki, T. Kakeshita, T. Ito, and S. Uchida, *Proc. Natl. Acad. Sci. U.S.A.* **108**, 12 238 (2011).
- ¹⁹ E. P. Rosenthal, E. F. Andrade, C. J. Arguello, R. M. Fernandes, L. Y. Xing, X. C. Wang, C. Q. Jin, A. J. Millis, and A. N. Pasupathy, *Nature Phys.* **10**, 225232 (2014).
- ²⁰ R. M. Fernandes, A. E. Böhmer, C. Meingast, and J. Schmalian, *Phys. Rev. Lett.* **111**, 137001 (2013).
- ²¹ H. Kontani, and Y. Yamakawa, *Phys. Rev. Lett.* **113**, 047001 (2014).
- ²² H. Kontani, T. Saito, and S. Onari, *Phys. Rev. B* **84**, 024528 (2011).
- ²³ A. E. Böhmer, P. Burger, F. Hardy, T. Wolf, P. Schweiss, R. Fromknecht, M. Reinecker, W. Schranz, and C. Meingast, *Phys. Rev. Lett.* **112**, 047001 (2014).
- ²⁴ A. E. Böhmer, T. Arai, F. Hardy, T. Hattori, T. Iye, T. Wolf, H. v. Löhneysen, K. Ishida, and C. Meingast, *Phys. Rev. Lett.* **114**, 027001 (2015).
- ²⁵ Y. Gallais, R. M. Fernandes, I. Paul, L. Chauviere, Y. X. Yang, M. A. Measson, M. Cazayous, A. Sacuto, D. Colson, and A. Forget, *Phys. Rev. Lett.* **111**, 267001 (2013).
- ²⁶ W. L. Zhang, P. Richard, H. Ding, Athena S. Sefat, J. Gillett, Suchitra E. Sebastian, M. Khodas, and G. Blumberg, arXiv:1410.6452 (2015).
- ²⁷ V. K. Thorsmolle, M. Khodas, Z. P. Yin, Chenglin Zhang, S. V. Carr, Pengcheng Dai, and G. Blumberg, arXiv:1410.6452 (2015).
- ²⁸ S. Caprara, C. Di Castro, M. Grilli, and D. Suppa, *Phys. Rev. Lett.* **95**, 117004 (2005).
- ²⁹ F. Kretzschmar, T. Böhm, U. Karahasanovic, J. Schmalian, and R. Hackl, (unpublished) (2015).
- ³⁰ Y. Gallais, I. Paul, L. Chauviere, and J. Schmalian, arXiv:1504.04570 (2015).
- ³¹ R. Applegate, R. R. P. Singh, C. C. Chen, and T. P. Devereaux, *Phys. Rev. B* **85**, 054411 (2012).
- ³² W. Lv, and P. Phillips, *Phys. Rev. B* **84**, 174512 (2011).
- ³³ S. Liang, A. Moreo, and E. Dagotto, *Phys. Rev. Lett.* **111**, 047004 (2013).
- ³⁴ C. C Lee, W. G. Yin, and W. Ku, *Phys. Rev. Lett.* **103**, 267001 (2009).
- ³⁵ F. Krüger, S. Kumar, J. Zaanen, and J. van den Brink, *Phys. Rev. B* **79**, 054504 (2009).
- ³⁶ W. Lv, F. Krüger, and P. Phillips, *Phys. Rev. B* **82**, 045125 (2010).
- ³⁷ P. Dai, J. Hu, and E. Dagotto, *Nature Phys.* **8**, 709-718 (2012).
- ³⁸ C. Fang, H. Yao, W. F. Tsai, J. P. Hu, and S. A. Kivelson, *Phys. Rev. B* **77**, 224509 (2008).
- ³⁹ C. Xu, M. Müller, and S. Sachdev, *Phys. Rev. B* **78**, 020501(R) (2008).
- ⁴⁰ A. V. Chubukov, D. V. Efremov, and I. Eremin, *Phys. Rev. B* **78**, 134512 (2008).
- ⁴¹ H. Yamase, and R. Zeyher, arXiv:1503.07646 (2015).
- ⁴² T. P. Devereaux, and R. Hackl, *Rev. Mod. Phys.* **79**, 175 (2007).
- ⁴³ S. Caprara, C. Di Castro, B. Muschler, W. Prestel, R. Hackl, M. Lambacher, A. Erb, S. Komiya, Y. Ando, and M. Grilli, *Phys. Rev. B* **84**, 054508 (2011).
- ⁴⁴ S. Caprara, C. Di Castro, T. Enss, and M. Grilli, *Journal of Magnetism and Magnetic Materials* **321**, 686-689 (2009).
- ⁴⁵ L. Tassini, F. Venturini, Q. M. Zhang, R. Hackl, N. Kikugawa, and T. Fujita, *Phys. Rev. Lett.* **95**, 117002 (2005).
- ⁴⁶ T. P. Devereaux, and A. P. Kampf, *Phys. Rev. B* **59**, 6411 (1999).
- ⁴⁷ B. Valenzuela, M. J. Calderon, G. Leon, and E. Bascones, *Phys. Rev. B* **87**, 075136 (2013).
- ⁴⁸ I. Paul, *Phys. Rev. B* **90**, 115102 (2014).
- ⁴⁹ T. P. Devereaux, D. Einzel, B. Stadlober, R. Hackl, D. H. Leach, and J. J. Neumeier, *Phys. Rev. Lett.* **72**, 396 (1994).
- ⁵⁰ S. H. Baek, D. V. Efremov, J. M. Ok, J. S. Kim, Jeroen van den Brink, and B. B. Büchner, *Nature Mat.* **14**, 210 (2015).
- ⁵¹ J. A. de Azcarraga, A. J. Macfarlane, A. J. Mountain, and J. C. Perez Bueno, *Nucl. Phys. B* **510**, 657-687 (1998).
- ⁵² J. A. de Azcarraga, and A. J. Macfarlane, *IJMPA* **16**, 1377-1405 (2001).